Development of a Cavity Ring-Down Spectroscopy Sensor for Boron Nitride Erosion in Hall Thrusters

IEPC-2009-146

Presented at the 31st International Electric Propulsion Conference,
University of Michigan • Ann Arbor, Michigan • USA
September 20 – 24, 2009

Lei Tao[1], Brian Lee[2] and Azer Yalin[3]
Colorado State University, Fort Collin, CO, 80521, USA

Naoji Yamamoto[4]
Kyushu University, Kasuga, Fukuoka, 8168580, Japan

and

Alec Gallimore[5]
University of Michigan, Ann Arbor, Michigan, 48109, USA

Abstract: Sputter erosion of boron nitride (BN) is a critically important process in many Hall thrusters from the point of view of both lifetime assessment and contamination effects. This contribution describes the development of a laser based sensor for *in situ* monitoring of sputtered BN from Hall thrusters. We present a laser electro-optic system and its demonstrative measurement results from BN sputtering experiments. A frequency-quadrupled diode laser at 250 nm is used as the light source for continuous-wave cavity ring-down spectroscopy. The optical cavity is mounted on a rail system and fiber optics are used to deliver light in/out of the vacuum chamber. Details of fiber optic delivery and future prism-based cavities are also discussed.

Nomenclature

A_{ki}	=	Einstein A coefficient
Abs	=	absorbance
c	=	speed of light
E_b	=	binding energy
f	=	focal length
g_i	=	degeneracy of state i
g_k	=	degeneracy of state k
I_b	=	ion beam current
$k(x,v)$	=	absorption coefficient
k_λ	=	imaginary component of the index-of-refraction
l	=	cavity length
M^2	=	beam quality factor

[1] Graduate Student, Department of Mechanical Engineering, lei.tao@colostate.edu
[2] Graduate Student, Department of Physics, blee66@rams.colostate.edu
[3] Associate Professor, Department of Mechanical Engineering, azer.yalin@colostate.edu
[4] Assistant Professor, Department of Advanced Energy Engineering Science, yamamoto@aees.kyushu-u.ac.jp
[5] Professor, Department of Aerospace Engineering, rasta@umich.edu

N_i = lower state concentration
R = mirror reflectivity
$S(t,v)$ = ring-down signal
t = time
V_b = ion beam voltage
x = position along the optical axis
λ = wavelength
v = laser frequency
v_{ki} = resonant frequency of transition from state i to k
τ = exponential decay time constant

I. Introduction

HALL thrusters are becoming increasingly widely used in space propulsion applications. The combination of high specific impulse, high thrust efficiency, and high thrust density makes the Hall thruster very attractive for many space missions. However, long operation times are usually needed to accomplish space missions and as a result long lifetimes are critical.[1,2] The primary lifetime limitation of Hall thrusters is sputter erosion of the acceleration channel wall. Sputter erosion not only leads to end of life, but also causes deposition of sputtered wall material and forms unwanted coatings on spacecraft surfaces such as solar arrays and sensor optics. Currently, thruster lifetimes are determined in ground-based life tests. With proposed thruster durations now as long as 5-10+ years, ground-based life tests are becoming increasingly impractical and expensive. In order to avoid the unacceptably risky alternative of doing no life testing, it is crucial to develop accelerated testing capabilities that allow rapid measurements of low sputter erosion rates. Such test capabilities could also aid in the understanding and optimization of Hall thruster design and operation. From the point of view of erosion (and contamination) in Hall thrusters, boron nitride (BN) is generally the material of primary interest as it is widely used as an insulator material in the acceleration channel of stationary plasma thrusters (SPTs). The low sputter erosion rates of BN combined with the need for *in situ* measurements severely limit the available diagnostic methods.

We have focused on the development of cavity ring-down spectroscopy (CRDS) as a non-intrusive *in situ* sputter diagnostic.[3-9] Previous research efforts have primarily demonstrated the use of CRDS to study sputtered metals (e.g. molybdenum, titanium and manganese) both for electric propulsion applications and for process control and monitoring in industrial sputter systems, including ion beam etch systems.[3-7] We have also pursued development of CRDS for measurement of BN.[8-9] The present contribution concerns our continued development of a CRDS senor to study *in situ* BN erosion in Hall thrusters by probing sputtered boron atoms at 250 nm. We have extended our past work to make the first cw-CRDS measurements of sputtered BN within a vacuum chamber. To allow stable operation within (large) vacuum chambers, the optical cavity is integrated with a portable rail system and light is fiber optically delivered in/out of the chamber. The lack of high reflectivity cavity mirrors at this wavelength poses sensitivity challenges for CRDS measurements in the targeted ultraviolet wavelength region. A prism-based CRDS system is currently in development with the goal of improving cavity finesse in the UV region, thereby increasing the sensitivity of BN detection.

Section II of this paper summarizes the CRDS technique, including the use of prism-based cavities. The details of our diagnostic test bed and demonstrative CRDS results are presented in Section III, along with initial prism characterization work. Section IV discusses chamber integration issues, including rail design and single-mode fiber delivery using photonic-crystal fibers. Finally, conclusions are given in Section V.

II. Cavity Ring-Down Spectroscopy (CRDS)

CRDS is an ultra-sensitive laser based absorption diagnostic, which has become a widely used method to do species-specific measurements in diverse applications including atmospheric monitoring, analytical chemistry, and combustion and plasma diagnostics.[10,11] Like other laser absorption methods, it is attractive because it can probe ground states, so a large fraction of the species population can be directly measured (in contrast to optical emission spectroscopy, which measures only small population factions of excited states). Relative to conventional laser absorption,[12] CRDS achieves enhanced sensitivity with detection limits as low as ~10^{-8}-10^{-11} cm^{-1} for ~1-10s measurement times.

A. CRDS Technique

The basic idea of CRDS is to place a high-finesse cavity, typically formed from a pair of high-reflectivity mirrors, around the absorbing species, as shown in Fig. 1. The probe laser beam is coupled into the optical cavity

where it is reflected back and forth many times, e.g. ~10^4 passes for mirror reflectivity of R~0.9999. Such a high number of passes through the cavity greatly increases the effective path length through the absorber, and thus greatly increases the absorption detection sensitivity. A detector placed behind the cavity measures the intensity of the light exiting the cavity, which is termed the ring-down signal. Under appropriate conditions, this signal decays exponentially with time.[13,14]

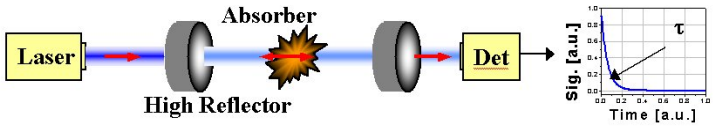

Figure 1. Schematic of CRDS experiment

$$S(t,\nu) = S_0 \exp\left[-t/\tau(\nu)\right]$$
$$1/\tau(\nu) = \frac{c}{l}\left[\int k(x,\nu)dx + (1-R)\right] \quad (1)$$

If an approximation is made that the sample is uniformly present along some column length l_{abs}, then $k(x, \nu)dx$ is equivalent to $k(x,\nu)l_{abs}$. The ring-down time τ is extracted by performing an exponential fit to the measured ring-down signal. The "empty cavity ring-down time" τ_0, (which we measure by detuning the laser from resonance) is used with $\tau(\nu)$ to calculate the sample absorbance, *Abs*, absorption coefficient.

$$Abs(\nu) \equiv \int k(x,\nu)dx = \frac{l}{c}\left[\frac{1}{\tau(\nu)} - \frac{1}{\tau_0}\right] \quad (2)$$

A typical method is to scan the laser frequency across the absorption line, thereby measuring the frequency (or wavelength) integrated spectrum. Using known spectroscopic parameters for a transition from a lower state *i* to an upper state *k*, the measured absorption line area $\int Abs(\nu)d\nu$, can be converted to the path-integrated concentration of the ground state $N_i dx$ *by:*

$$\int N_i dx = 8\pi \frac{g_i}{g_k}\frac{\nu_{ki}^2}{A_{ki}c^2}\left(\int Abs(\nu)\,d\nu\right) \quad (3)$$

The above discussion has not included longitudinal and transverse modes of the cavity.[15,16] When performing CRDS with a typical pulsed-laser having a spectral bandwidth of ~1-10 GHz (p-CRDS), there is usually no need to worry about the mode structure since the laser linewidth is large relative to typical cavity-mode spacing. However, in p-CRDS due to this multimode excitation, the mode structure causes mode beating[13,17] that can generate oscillations in the ring-down transient, which leads to inaccuracy and reduced sensitivity in measurements. An alternative, as we employ, is to use a continuous-wave laser with a much smaller bandwidth (typically ≤1-10 MHz). In this scheme, called continuous-wave cavity ring-down spectroscopy (cw-CRDS), one excites a single longitudinal mode of the optical cavity and achieves much better sensitivity.[15,16] This is extremely important for detecting very low concentrations of particles, especially in wavelength regions where available mirror reflectivities are not so high, as is the case in measurement of sputtered BN (boron atoms) from Hall thrusters. Moreover, cw-CRDS has a higher repetition rate and higher spectral resolution, which allows us to perform near real-time measurements and study the hyperfine structures of atoms and molecules.

B. Prism Based CRDS

In almost all forms of CRDS, dielectric mirrors are used to create high finesse optical cavities. High reflectivity is achieved with multilayer coatings that cause constructive interference of the Fresnel reflections. This approach is quite effective for wavelengths ranging from the near-UV to the mid-IR, allowing mirror losses of less than 100 parts per million (ppm). However, these reflectivities degrade as one moves further into the UV region owing to absorption of light within the coating layers. For 250 nm light (specific to boron nitride detection) 99.8% is the best available reflectivity we have seen from commercially available dielectric mirrors. In parallel with our studies using conventional dielectric mirrors, we are also researching novel prism-based cavities to enable lower cavity loss and improved detection sensitivity.

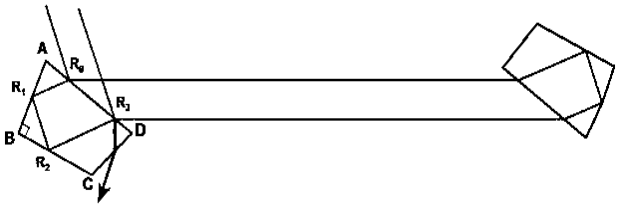

Figure 2. Schematic for a prism-based optical cavity.

The basic idea of the prism cavity is to use a pair of Brewster's angle prisms constructed from calcium fluoride (CaF_2) that use total internal reflection to give high reflectivity in the UV region. Such a cavity has already been demonstrated in the visible and NIR regions using fused silica.[18] Pipino *et al.* previously demonstrated evanescent wave absorption CRDS using total internal reflection within a single prism.[19] In our proposed system, two CaF_2 prism retroreflectors are faced towards each other, forming a stable ring cavity as shown in Fig. 2. Light is coupled into and out of the cavity at R_3 and R_0 respectively. The beam undergoes total internal reflection at R_1 and R_2. Side AD is placed at Brewster's angle to minimize reflected losses. One of the total internal reflection surfaces will be curved in order to add a focusing element to the cavity.

In addition to low reflectivity in the UV region, dielectric mirrors are limited by the narrow bandwidth over which they can perform, often <5-10% of the center wavelength. Total internal reflection, and therefore a prism retroreflector, provides high reflectivity over all wavelengths as long as the critical angle condition is met and the prism losses are low. This opens the possibility for broadband CRDS with a single experimental setup, allowing for simultaneous species detection with high sensitivity.[20] Such a capability could allow simultaneous detection of multiple sputtered species.

III. Experimental

A. Diagnostic Apparatus

The primary component of the CRDS sputter measurement system is a sputtering apparatus within a vacuum chamber containing an optical rail system. Figure 3 shows a schematic diagram of the diagnostic apparatus emphasizing non-optical aspects. With roughing and turbo pumps (Turbo-V550), the pressure inside the vacuum chamber reaches approximately 10^{-6} Torr under no-flow conditions and 10^{-5} Torr under a small feeding argon flow (~2.5 sccm) for the ion source. At these conditions, the sputtered atoms are in a free-molecular regime (Knudsen number << 1). The ion beam is extracted from an 8 cm diameter structurally integrated two-grid ion source using refractory metal filaments for both the main and neutralizer cathodes. The ion source operates with an IonTech power supply (MPS 3000), with typical beam currents and voltages of about 10–100 mA and 400–1200 V respectively. The target, currently a piece of BN (15 cm long, 12 cm wide), is mounted on a stainless steel post and is (approximately) normal to the ion beam. It is located 20 cm away from the ion source exit. The BN sample is HBC grade from General Electric's Advanced Ceramics. Due to the divergence of the ion beam from our ion source, only 10% beam current is measured to hit the target.

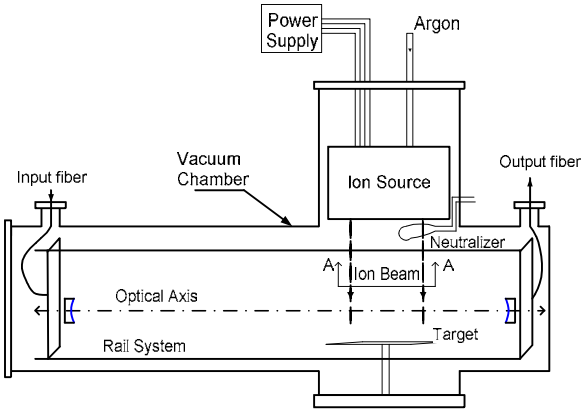

Figure 3. Schematic diagram of diagnostic apparatus

B. cw-CRDS Setup

Compared to the p-CRDS setup,[3-6] the increased complexity of the cw-CRDS setup arises due to the dependence of the spectral overlap between the optical cavity modes and the probe laser.[15,16] Figure 4 shows a schematic diagram of our cw-CRDS setup. A frequency-quadrupled external cavity diode laser system with a spectral bandwidth less than 5 MHz (Toptica TA-FHG110) is used as the continuous-wave light source that can generate a 60 GHz mode-hop free tuning range around the transition lines of boron at 249.753 nm and 249.848 nm, with output power ~10 mW. The targeted lines are selected based on their optical accessibility and high absorption strength. A beam splitter is placed in front of the laser and sends about 10% of the laser power through a solid etalon (UV enhanced fused silica solid Fabry–Pérot etalon, finesse of ~10 at 250 nm) and onto a photodetector in order to generate a frequency reference signal. The rest of the laser beam goes though an acousto-optic modulator (AOM) after focusing with a lens. The AOM is used as a fast optical switch with a threshold detection circuit to extinguish the laser beam once the output signal reaches a certain threshold. Only the first order output beam (~70% of the input laser power) from the AOM is used. This portion of the beam is coupled into the vacuum chamber using a 4 m long large mode area photonic-crystal fiber (PCF) with a core diameter of ~10μm (Crystal Fibre LMA-10 UV), giving a single mode beam, details of the PCF delivery are given in Section IV. At the output of the PCF, two plane-convex fused silica lenses (f =20 mm, f =500 mm) are used to maximize the coupling of the laser beam to the

(fundamental) longitudinal mode (TEM_{00}) of the cavity. The optical cavity has length of 75 cm and is formed by a pair of high reflectivity mirrors each 2.54 cm in diameter with a 1 m radius of curvature. An empty-cavity ring-down time around 1.3 μs is achieved, corresponding to R ~99.80% (2000 ppm loss). The BN target is placed parallel with the optical axis with a 1 cm offset. Behind the cavity, the output beam is coupled into a UV multimode fiber (OZ optics, QMMJ-3s3s-UVVIS) that delivers light to a photomultiplier tube (Hamamatsu R9110 with a DA-type socket C7247) with a dielectric interference filter in front to suppress background light. All measurements are made by scanning the laser wavelength; ring-down signals are measured each time the laser spectrally overlaps with a cavity transmission peak. In other words, the ring-down acquisitions are spaced by the cavity free spectral range. Once the laser spectrally overlaps with a cavity transmission peak, an increase in the photomultiplier signal is observed and monitored by the threshold detection circuit that triggers the AOM to extinguish the incoming laser beam. The light inside the cavity then exponentially decays and generates a ring-down signal. A computer with a 20 MHz, 12 bit analog-to-digital acquisition board (Adlink PCI-9812/10) collects signals when triggered by the threshold detection circuit. A custom LABVIEW program is used for laser frequency calibration and exponential fitting (with the nonlinear Levenberg-Marquartdt fit).

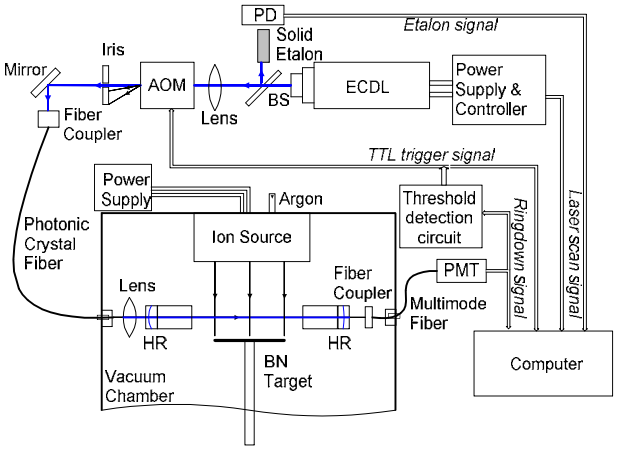

Figure 4. Schematic diagram of cw-CRDS setup: AOM-acousto-optic modulator, BS-beam splitter, ECDL-external cavity diode laser, HR-high reflectivity mirror, PD-photo detector, PMT-photomultiplier tube.

C. Demonstrative Measurements

The detection scheme for measurement of BN sputtering is to probe boron atoms in the ultraviolet. Details of the sputter product composition of BN are not fully understood,[21] but mass-balance considerations and past work indicate that the majority of sputtering is in the form of boron and nitrogen atoms (perhaps with a small fraction of BxNy clusters). It is also possible that the sputtered nitrogen is in the form N_2 or N_x, but this does not affect our measurements. Figure 5 shows resonance lines of neutral atomic boron from the ground state. Atomic boron has two distinct (fine-structure) ground states (J = 1/2 and 3/2) that result in two distinct absorption lines (249.753 nm and 249.848 nm). These lines have been selected owing to their combination of optical accessibility and relatively high strength. In all the experiments, the diode laser system was tuned to scan ~55 GHz mode-hop free around 249.848 nm, which is the stronger absorption line. One scan takes about 12 s (up and down). The free spectral rang of the 75 cm cavity is approximately 200 MHz, giving approximately 550 ring-down events per scan.

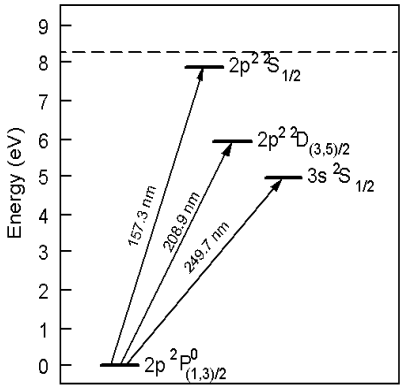

Figure 5. Boron atomic spectral lines

Figure 6 shows an example of measured boron spectrum with 20 s collection time with a beam current of 50 mA and beam voltage of 1200 V. The absorbance spectrum is plotted in units of parts per million (referring to the absorbance not sample concentration). To construct the spectrum, we used a binning approach in which the frequency axis was divided into a series of bins, each with a width of 1 GHz. Within each bin, the experiment data points were averaged both by frequency and ring-down time. A Voigt profile was fitted to the experiment data points. As discussed above Eq. (3), the path-integrated concentrations were from the wavelength-integrated area of the spectrum. The true lineshape is not Voigt, but the Voigt lineshape provides a convenient means to fit data and determine the area.

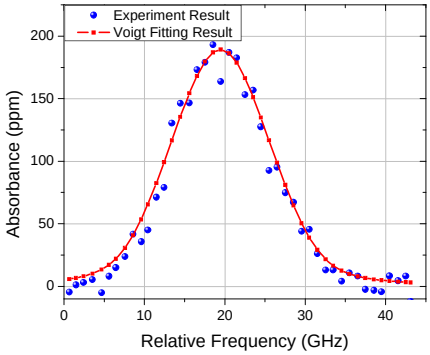

Figure 6. Boron absorbance spectrum for I_b=50mA, V_b=1200V

Initial tests were made to validate our cw-CRDS measurements. Several measurements of the number density were made as the beam current and voltage were varied. Figure 7(a) shows a plot of the dependence of path-integrated boron number density on the ion voltage. The ion beam voltage was kept at 1200V, while the ion beam current varied from 30 mA to 60 mA. The sputter yield per incident ion does not change with beam current density. Therefore, the path-integrated number density of boron is expected to be proportional to the beam current and we find the correlation coefficient R > 99.8% from linear fitting. Figure 7(b) shows a plot of dependence of path-integrated boron number density on the ion beam voltage. The sputter yields per incident ion changes almost linearly in this voltage range and again the path-integrated number density shows good linearity with a correlation coefficient R > 99.80%. Both of these results contribute to validation of the basic performance of the cw-CRDS sensor.

As described in our previous work[3-6], a mathematical model for analyzing the CRDS sputtering signals has been made with a finite element approach. Table 1 shows the comparison between actual measured number density and the calculated number density from our finite element model, where the beam voltage is 1200V and beam current is varied. We assume a uniform current density distribution on the target, a diffuse shaped sputter yield, and adopt the binding energy E_b = 3.865 eV (v_b = 8300 m/s)[8] with an exponent of 1.8 in the Thomson distribution for particle velocity. The sputter yield for BN at 1200 V is interpolated from BN sputter yield results.[9] The uncertainty on the experimental value is from Einstein A coefficient and reproducibility of the measurements, while the uncertainty in the model (± 44%) has contributions from total sputter yield (± 30%), shape of differential sputter yield (± 5%), velocity distribution (± 30%), and current density distribution (± 12%). There is favorable agreement (within error bars) between the model and experiment. Future efforts will include experimental measurement of the sputtered particle velocity distribution, both by CRDS[6] and Laser induced fluorescence. The latter technique has been extensively demonstrated for velocity measurements of sputtered particles.[22] Knowledge of particle velocity is also needed to relate CRDS number densities to particles fluxes, as is needed to infer thruster erosion rates from the CRDS results.

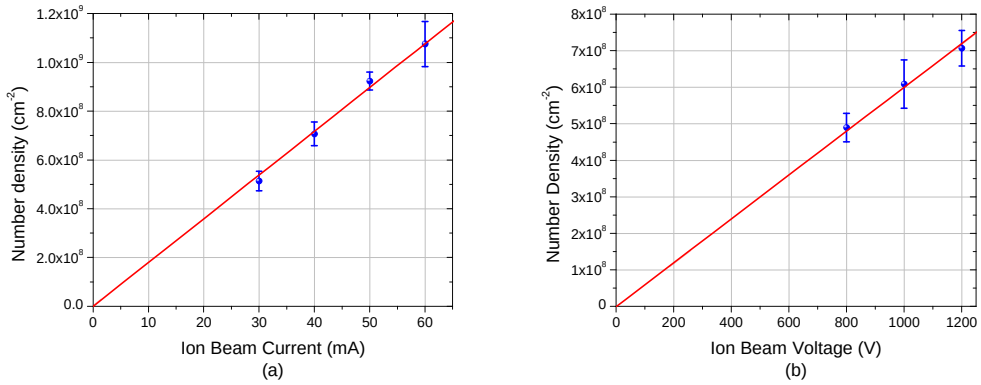

Figure 7. (a) Dependence of path-integrated boron number density on the ion beam current at V_b = 1200V. b) Dependence of path-integrated boron number density on the ion beam voltage at I_b = 40mA

Beam Current, mA	cw-CRDS Number Density, cm^{-2}	Finite Element Model Number Density, cm^{-2}
30	$5.1 \pm 0.4 \times 10^8$	$9\pm 4\times 10^8$
40	$7.1 \pm 0.5 \times 10^8$	$12 \pm 5 \times 10^8$
50	$9.2 \pm 0.5 \times 10^8$	$15 \pm 7 \times 10^8$
60	$10.8 \pm 0.9 \times 10^8$	$18 \pm 8 \times 10^8$

Table 1. Measured and modeled boron number density for V_b = 1200V

Estimates of minimum detectable absorbance can be found from the noise in the cw-CRDS detection system. The minimum detectable absorbance, Abs_{Min}[13], is calculated from:

$$Abs_{Min} \equiv \frac{\Delta\tau}{\tau}(1-R) \tag{4}$$

where $\Delta\tau$ is the uncertainty (noise) in measurement of ring-down time τ, for which we use the standard error in measurement of τ. The standard error represents the expected standard deviation between the measured estimates and the true value, and is computed as the standard deviation divided by the square-root of the number of measurements. The standard deviation of the cw-CRDS system is approximately 1% of ring-down time τ. For a fixed frequency, the minimum detectable absorbance is about 0.6 ppm in 20 s measurement time (~1000 ring-down events). For a scanned frequency, there are about 20 ring-down measurements within each 1 GHz bin in 20 s. The minimum detectable absorbance for BN is about 5 ppm in 20 s measurement time. These detection limits compare favorable with those of our past work and those needed for measurements at expected thruster conditions.[9] Use of prism cavities with improved reflectivities, should further increase sensitivity,.

D. Prism Characterization

As discussed above, we are pursuing a parallel effort to increase BN detection sensitivity though the use of high-finesse optical cavities based on calcium fluoride prisms as retro-reflectors. Given the unique nature of these prisms, and the extremely high quality needed in their construction, it is important to understand the optical losses that can be expected from CaF_2 made by different vendors. To test this we have obtained four super-polished CaF_2 samples (~0.1 nm or less in microroughness) from different vendors. These cylindrical samples have the same dimensions with the front and back surfaces highly polished. By measuring the transmission through the samples at a variety of points, the quality of the different samples can be compared. This may also give more insight into the optical loss mechanisms that occur in CaF_2 and therefore in the prism retro-reflectors.

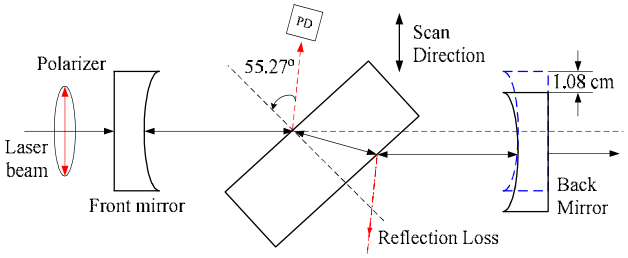

Figure 8. Setup for measuring the optical transmission of a CaF_2 sample within a dielectric mirror cavity.

Due to the very low optical loss in CaF_2, a CRDS measurement scheme is used for the loss measurements. The experimental setup for measuring the optical loss of a CaF_2 sample is shown in Fig.8. Each sample is a cylinder 2.54 cm thick and 5.08 cm in diameter. This thickness was chosen such that the path length within the sample is nearly the same as within the prisms. The sample is placed within the optical cavity as a "loss element" at Brewster's angle. A photodiode is used to measure the reflected loss at the surface, such that Brewster's angle can be optimized. The back cavity mirror must be translated due to the horizontal displacement in the beam when the sample is present. A three-axis translation stage allows the sample to be translated while the ring-down time is being measured, scanning the beam across the surface. The losses from example scans at 403 nm and 250 nm are shown in Fig. 9.

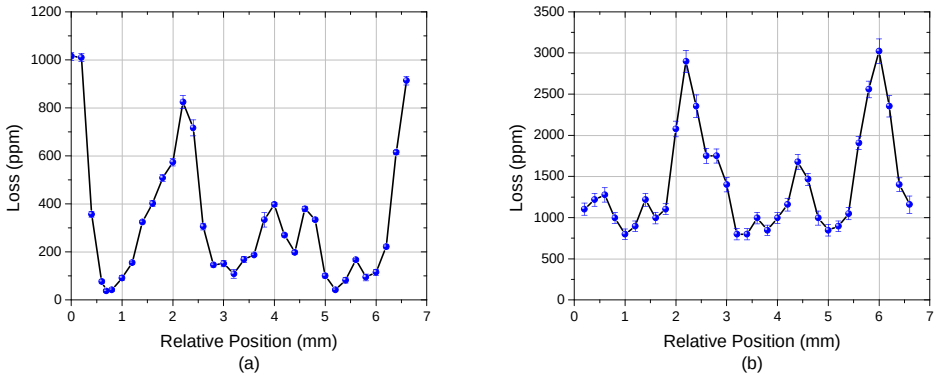

Figure 9. Optical loss through a CaF_2 sample placed at Brewster's angle at (a) 403 nm and (b) 250 nm.

These scans show that the CaF_2 is capable of having high transmission in both the UV and visible regions. Transmissions as high as 99.99% and 99.9% have been regularly observed at 403 nm and 250 nm respectively. In some cases, transmission as high as 99.95% have been measured at 250 nm, corresponding to losses about 5 times lower than the best dielectric mirrors available to us. Note that optical transmission in this context is approximately analogous to reflectivity for a dielectric mirror. The only additional loss that the prisms are likely to incur that is not being measured here is the loss associated with total internal reflection, which is expected to be low. Concerns remain about the consistency of the surfaces, as is evident in the large fluctuations in loss with position. However, these results give encouragement that the prisms can out-perform the dielectric mirrors at a particular wavelength in the UV region and certainly with a broadband spectrum.

IV. Chamber Integration

A. Rail System

An optical rail system is a custom designed self contained unit that holds all optics together inside the vacuum chamber. As shown in Fig. 10, the rail system includes custom made aluminum wall plates connected by carbon fiber rods and mounted to a base plate. The three carbon fiber rods have a nearly zero coefficient of thermal expansion (0 CTE), which helps prevent optical misalignment from rod deflecting under the intense heat loading of the Hall thruster (or ion source). The wall plates are designed to slide axially along the three rods, allowing for an adjustable cavity length. On these wall plates, a 30 mm optical cage system is mounted to house all optics, including fiber connector, alignment optics, high reflectivity mirrors. In order to protect the mirrors from sputter deposition, two 10 cm long tubes containing a series of 2 mm irises inside are mounted to the wall plates in front of each mirror. This allows us to have a longer operation time (tens of hours) with minimal degradation of mirror reflectivity, which causes reduction in detection sensitivity.[7] Under the base plate, four rubber damping feet are used to minimize vibrations, especially from the pump system. Two custom made feed-throughs for the multimode fiber and PCF help deliver the fibers in the chamber and seal the vacuum.

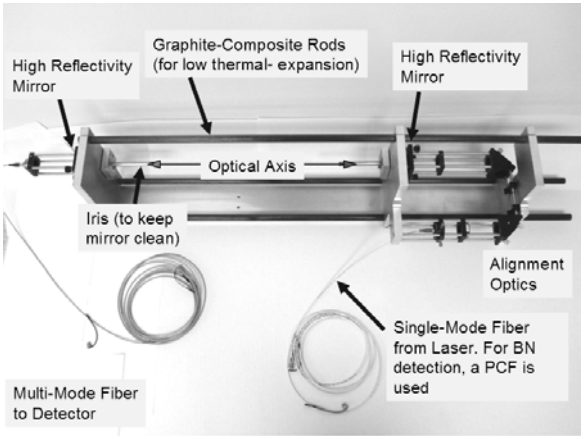

Figure 10. Fiber-coupled rail for implementation within vacuum chamber

The advantage of such a modular design is that experiments can be conducted in various vacuum facilities with little or no modification. Moreover, the rail system allows for the optical setup to be tested and adjusted outside of the vacuum chamber, and maintains alignment as the chamber is pumped down. This is in contrast to our past efforts[3-6] in which the cavity mirrors were mounted on the outer walls of the vacuum chamber and suffered from alignment degradation as the chamber was pumped down or heated (and the walls deflected).

In actual Hall thruster tests, the rail system needs to be close to the thruster's exit plane (with the optical axis across the thruster plumes), i.e. in a position where radiation (including a lot of UV light) is present. Intense UV light causes damage to the dielectric multi-layer coated mirrors, which leads to the degradation of reflectivity.[23] Even though irises can help to reduce UV light exposure, the high reflectivity mirrors still suffer from UV light radiation, which causes reduction of ring-down time (measurement sensitivity). The magnitude of these effects and possible counter measures will be studied in future work. A prism-based cavity may help to prevent such damage since there is no multi-layer coating on the prism.

B. Fiber Delivery with Photonic Crystal Fibers

Fiber delivery provides great flexibility in handling the laser light in harsh environments. For the CRDS erosion sensor, delivery of UV light into the vacuum chamber by optical fibers is strongly desirable, as it avoids many complications associated with cavity mirrors mounted on the wall and delivery mirrors external to the vacuum chamber. Certain fiber optics also allows single-mode output as required for cw-CRDS. However, the choice of available waveguides for this purpose is limited. In terms of widely available single-mode silica step-index fibers, the shortest cutoff wavelength is ~300 nm with core diameter of ~2 μm for delivery of 250 nm light. For our laser system with these parameters, it is almost impossible to get reasonable input coupling and transmission efficiency (output power). As we have recently shown, the use of photonic crystal fibers (PCFs) is for single-mode delivery of

UV wavelengths.[24] Typical PCFs have a uniform patterned microstructure of holes (defects) running axially along the fiber channel with a missing hole in the center providing a core region. With appropriate fiber design, the fiber core can support a single guided mode over all optical frequencies, a characteristic referred to as "endless single-mode operation."

In our setup, a large mode area (LMA) PCF is employed and, as will be discussed, we obtained single mode output with reasonable transmission efficiency (~ 45% for 1 m PCF) over a short distance <10 m. We use LMA PCFs with a core diameter of ~10 μm. These fibers are optimized for ultraviolet and visible operation.[25] The fibers have a single cell triangular structure with lattice spacing (pitch) of 6.26 μm and a hole size of 3.04 μm. Modeling shows them to be endlessly single-mode. The overall cladding diameter is ~230 μm. For 250 nm operation, the fiber NA and mode field diameter (MFD) are estimated as ~0.03 and ~8 μm respectively. We have done some measurements with end-sealed fibers, but results reported here are primarily for unsealed fibers. The end faces have been cleaved but not prepared in other ways.

With proper alignment, single mode output can be achieved from the PCF.[24] Figure 11 shows a photograph of the fiber output incident on a card several cm downstream of the fiber exit. The shape of the beam pattern is typical of single-mode output from a triangular PCF.[26] The single-mode output was also confirmed in several ways. First, we checked power transmission through a downstream pinhole. We used a first lens to collimate the fiber output to diameter 0.8 mm and then a second lens of focal length 45 mm to focus the light through a pinhole. In this way, we could transmit more than 90% of the power through a 30 μm pinhole. Second, we have mode matched the fiber output to our high-finesse CRDS optical cavity and coupled the light predominantly to the fundamental longitudinal cavity modes (higher order modes exiting the fiber would couple to higher order cavity modes). The cw-CRDS results of Section III used the PCF for fiber delivery. Finally, we have used a Spiricon beam profiler (SCOR20) to measure the M^2 of the light exiting the fiber (length 1.3 m). The output beam was weakly focused using a plano-convex lens (focal length 20 mm) and the dependence of beam diameter on position resulted in M^2=1.08, confirming (near) single-mode output.

Figure 11. Photograph of single-mode output beam from PCF.

The transmission and bend properties of this PCF were also measured for operation at 250 nm.[24] Rather than performing a cutback test, we studied the fiber coupling and transmission loss by measuring the power transmission for fibers of several lengths. Figure 12 shows the results for fibers of length 0.45-4 m. The power at the fiber input was ~1 mW. For testing for fiber lengths of <3 m the fiber was held relatively straight, while for testing for lengths of >=3 m the fiber was moderately bent with radius of curvature of roughly 0.5 m. Fiber bend loss is further discussed below. The transmission data are reasonably fit (correlation coefficient R= 0.96) with a straight line of intercept -1.8 ± 0.6 dB and slope of -1.5 ± 0.2 dB/m, corresponding to a coupling loss of ~34% and transmission loss of ~29% loss per meter. The scatter in the data may be due to optimization of alignment for each fiber, but is also likely related to optical damage discussed below. The observed coupling loss is reasonable for single-mode coupling at these short wavelengths, though some optimization may be possible with better mode matching (e.g. reduction of aberration or improved combination of launch lens and beam diameter). The transmission loss can be converted to a (Beer's Law) absorption coefficient of a_λ=0.35 ± 0.05 m^{-1}. To find the corresponding absorption index k_λ, we use $k_\lambda=(\lambda/4\pi)a_\lambda$ where λ is the (free-space) wavelength, and find k_λ= (7 ± 1) x 10^{-9}. The value is somewhat low relative to published values for silica glass[27], but there is considerable scatter and uncertainty in these measurements owing to the type of silica (natural versus synthetic), impurities, and measurement method (e.g. transmission based measurements cannot adequately resolve small losses). Another comparison can be made with extrapolation of the fiber data-sheet[25] using a λ^{-4} scaling (i.e. assuming loss is dominated by Rayleigh scattering) which gives ~0.25 dB/m (k_λ=1.2x10^{-9}) indicating that there is an additional absorption contribution, likely from impurities (e.g. Cl) and microbending

We also considered fiber bending loss. Fiber transmission was measured for a fiber with a single-loop (360° of bending) of different curvatures. The upstream and downstream segments of the fiber were held approximately straight. The bend loss results are shown in Fig. 13 and are determined from the additional transmission loss caused by bending. We find a critical bend radius of approximately 6 cm.

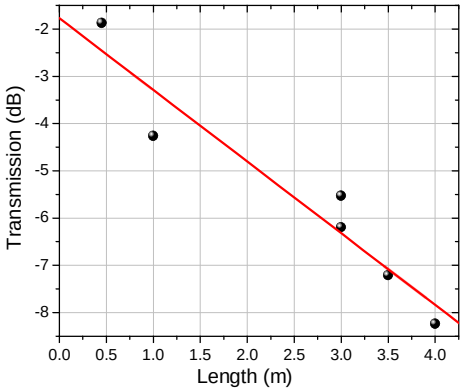

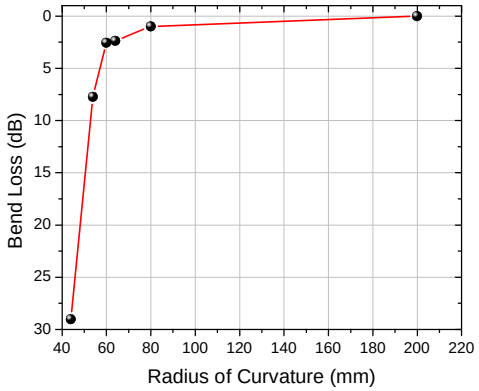

Figure 12. Fiber transmission loss versus fiber length Figure 13. Fiber bend loss versus radius of curvature

Optical damage of silica by UV photons[24,28,29] also provides a practical impediment to fiber delivery in this wavelength range. We have observed such effects in our experiment which, depending on laser power, lead to damage (reduced transmission) after 1 s - 10 s of hours. For input power of 0.3 mW, the damage is reduced with a decrease in transmission of <40% over more than 40 hours of operation. We also observed that cleaving the fiber input (tip) partially restores fiber transmission.[24] Clearly the optical damage is challenging in long-term applications (e.g. communication links), but the PCFs do allow sufficient operation times for our cw-CRDS BN sensor where typical measurement campaigns to study several thruster operating conditions require approximately one to several hours.

V. Conclusion

Boron nitride erosion limits the lifetime of SPTs and can cause contamination effects. Although several optical and non-optical erosion measurement techniques exist, there is a dearth of techniques that can provide sensitive quantitative measurements *in situ*. The CRDS sensor presented here contributes to addressing this need. In this work, a CRDS based boron nitride sensor has been developed based on cw-CRDS absorption of boron atom at 250 nm using a frequency-quadrupled diode laser. We have summarized the cw-CRDS measurement technique and the setup of our diagnostic test bed. We have presented validating measurements of boron concentration versus ion beam current and voltage. The sensor allows an absorbance detection limit of 5 ppm in 20 s which is expected to be adequate for thruster studies. Beam delivery using single-mode PCFs and future prism-based cavities have also been discussed. Initial tests of CaF_2 samples suggest that the prisms can outperform the dielectric mirrors at a particular wavelength in the UV region and certainly with a broadband spectrum. Upcoming work includes integration of the CRDS sensor with a Hall thruster test facilities and implementation of prism-based CRDS.

References

[1]Garner, C. E., Polk, J. E., Goodfellow, K. D., and Brophy, J. R., "Performance Evaluation and Life Testing of the SPT-100," *Proceedings of the 23rd International Electric Propulsion Conference*, IEPC paper 93-091, Electric Rocket Propulsion Society, Sept. 1993.

[2]Garner, C. E., Brophy, J. R., Polk, J. E., and Pless, L. C., "A 5730-Hr Cyclic Endurance Test of the SPT-100," *31st AIAA Joint Propulsion Conference*, AIAA paper 95-2667, July 1995.

[3]Surla,V., Wilbur, P.J., Williams, J.D., Johnson, M., and Yalin, A.P., "Sputter Erosion Measurements of Titanium and Molybdenum by Cavity Ring-Down Spectroscopy," *Review of Scientific Instruments*, Vol. 75, No. 9, 2004, pp. 3025-3030.

[4]Yalin, A.P., Surla, V., Butweiller, M., and Williams, J.D., "Detection of Sputtered Metals using Cavity Ring-Down Spectroscopy," *Applied Optics*, Vol. 44, No. 30, 2005, pp. 6496-6505.

[5]Yalin, A.P., and Surla, V., "Determination of Number Density and Velocity of Sputtered Particles by Cavity Ring-Down Spectroscopy," *Proceedings of the 29th International Electric Propulsion Conference*, IEPC paper 2005-300, Electric Rocket Propulsion Society, 2005.

[6]Yalin, A.P., and Surla, V., "Velocity Measurements by Cavity Ring-Down Spectroscopy," *Optics Letters*, 30, 2005, pp. 3219-.

[7]Tao, L., Yamamoto, N., Yalin, A.P., "Cavity Ring-Down Spectroscopy Sensor for Ion Beam Etch Monitoring and End-Point Detection of Multilayer Structures," *Review of Scientific Instruments*, 79, 115107, 2008.
[8]Yalin, A.P., Tao, L., Yamamoto, N., Smith, T.B., and Gallimore, A.D. "Boron Nitride Sputter Erosion Measurements by Cavity Ring-Down Spectroscopy," *30th International Electric Propulsion Conference* (Florence, Italy) 2007.
[9]Yalin, A.P., Tao, L., Sullenberger, R., *et al.*, "High-Sensitivity Boron Nitride Sputter Erosion Measurements by Continuous-Wave Cavity Ring-Down Spectroscopy," *44th AIAA Joint Propulsion Conference*, AIAA-2008-5091, Hartford, CT, USA, 2008.
[10]Busch, K. W., and Busch, M. A., *Cavity-Ringdown Spectroscopy*, Oxford University Press, Oxford, 1999.
[11]Berden, G., Peeters, R., and Meijer, G., "Cavity Ring-down Spectroscopy: Experimental Schemes and Applications," *International Reviews in Physical Chemistry*, Vol 19, 2000, pp. 565-607.
[12]Yamamoto, N., Yokota, S., Matsui, M., Komurasaki, K., and Arakawa, Y., "Measurement of Erosion Rate by Absorption Spectroscopy in a Hall Thruster," Review *of Scientific Instruments*, 76, Issue 8, 083111, 2005.
[13]Zalicki, P., and Zare, R.N., "Cavity ring-down spectroscopy for quantitative absorption measurements," *Journal of Chemical Physics*, Vol. 102, No. 7, 1995, pp. 2708-2717.
[14]Yalin, A.P., and Zare, R.N., "Effect of Laser Lineshape on the Quantitative Analysis of Cavity Ring-Down Signals," *Laser Physics*, Vol. 12, No. 8, 2002, pp. 1065-1072.
[15]Paldus, B.A, and Kachanov, A.A, "An Historical Overview of Cavity Enhanced Methods," *NRC Research Press Website @ http:// cjp.nrc.ca/*, Oct. 2002.
[16]Dudek, J.B, *et al.* "Trace Moisture Detection Using Continuous-Wave Cavity Ring-Down Spectroscopy," *Analytical Chemistry*, Vol. 75, Sept. 2003, pp. 4599-4605.
[17]Lehmann, K. K., and Romanini, D., "The Superposition Principle and Cavity Riong-down Spectroscopy," *Journal of Chemical Physics*, 105, 1996, pp. 10263-10277.
[18]Engel, G., Yan, W. B., Dudek, J. B., Lehmann, K. K., and Rabinowitz, P., "Ring-down spectroscopy with a Brewster's angle prism resonator," *Laser Spectroscopy XIV International Conference*, edited by R. Blatt, J. Eschner, D. Leibfried, and F. Schmidt-Kaler, World Scientifc, Singapore, 1999, pp. 314-315.
[19]Pipino, A. C. R., Hudgens, J. W., and Huie, R. E., "Evanescent wave cavity ring-down spectroscopy with a total-internal reflection minicavity," *Review Of Scientific Instruments*, Vol. 68, No. 8, August 1997, pp. 2978-2989.
[20]Johnston, P. S. and Lehmann, K. K., "Cavity enhanced absorption spectroscopy using a broadband prism cavity and a supercontinuum source," *Optics Express*, Vol. 16, No. 19, September 2008.
[21]Rubin, B., Topper, J., and Yalin, A.P., "Total and Differential Sputter Yields of Boron Nitride Measured by Quartz Crystal Microbalance", *submitted for publication to the 31st International Electric Propulsion Conference*, Ann Arbor, MI, 2009.
[22]Lucht, R. P., "Applications of laser-induced fluorescence spectroscopy for combustion and plasma diagnostics," in Laser Spectroscopy and Its Applications, L. J. Radziemski, R. Solarz, and J. A. Paisner, eds., Dekker, New York, 1987, Chap. 9, pp. 627.
[23]Yasumoto, M., Tomimasu, T., Nishihara, S., and Umesaki, N., "Optical damage of multi-layer mirrors for UV-FEL resonator induced with intense pico-second pulse FELs and Nd:YLF lasers" *Optical Materials* Vol. 15, 2000.
[24]Yamomoto, N., Tao, L., and Yalin, A. P., "Single-mode delivery of 250 nm light using a large mode area photonic crystal fiber," *Optics Express*, Vol. 17, 2009, pp. 16933–16940.
[25]Crystal Fiber: http://www.crystal-fibre.com/datasheets/LMA-10-UV.pdf Accessed on Jan. 30, 2009.
[26]Mortensen, N.A., and Folkenberg, J.R., "Near-field to far-field transition of photonic crystal fibers: symmetries and interference phenomena," *Optical Express*, Vol. 10, 2002, pp. 475-481.
[27]Kitamura, R., Pilon, L., and Jonasz, M. "Optical constants of silica glass from extreme ultraviolet to far infrared at near room temperature," *Applied Optics*, Vol. 46, 2007, pp. 8118-8133.
[28]Schenker, K.R., Schermerhorn, P., and Oldham, W.G., "Deep-ultraviolet damage to fused silica," *Journal of Vacuum Science & Technology B*, Vol. 12, 1994, pp. 3275-3279.
[29]Hillrichs, G., Dressel, M., Hack, H., Kunstmann, R., and Neu, W., "Transmission of XeCl Excimer Laser Pulses Through Optical Fibers: Dependence on Fiber and Laser Parameters," *Applied Physics B*, Vol. 54, 1992, pp. 208-215.